LIQUID FLOW THROUGH HOLES IN THE WALL OF A DIRECT-FLOW CENTRIFUGAL COMPONENT

V. A. Markov, A. M. Volk, and A. I. Ershov

UDC 621.928.38

Theoretical and experimental researches are reported for characteristics affecting the liquid flow during separation from a spiral gas–liquid stream in a centrifugal separator. Formulas are derived for the flow coefficient and pressure difference at the inner and outer sides of the wall.

High efficiency in phase interaction in a mass-transfer apparatus having an elevated gas load requires [1] a device for separating the liquid from the gas–liquid mixture. Such a device is necessary to prevent liquid carry-over between plates, which has an adverse effect on the mass transfer driving force. The separation also provides additional contact between the liquid and gas, which improves the mass transfer.

A device giving the maximum separation may be based on centrifugal forces arising from the rotation of the flow provided by various types of static spiralizer [2], including centrifugal separators as shown schematically in Fig. 1, in which there is a cylindrical tube 1 containing blade spiralizers 2 in the lower part and a separation zone in the upper one. The spiraling mixture is separated into gas and liquid, with the latter transported by the gas up the wall, where it is tapped off through the circular holes 3 (Fig. 1a) or the slots 4 (Fig. 1b). Efficient operation is dependent on what amount of liquid is separated by each row of holes. The flow through the holes can be calculated for a known pressure dif-

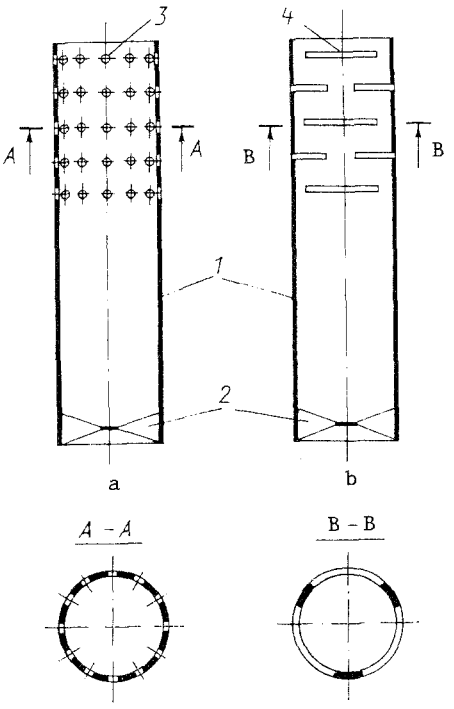

Fig. 1. Centrifugal separating elements having circular holes (a) or slots (b): 1) cylindrical tube; 2) vorticizer; 3) circular holes; 4) slots.

Kirov Belorussian Technological Institute, Minsk. Translated from Inzhenerno-Fizicheskii Zhurnal, Vol. 61, No. 1, pp. 82-87, July, 1991. Original article submitted July 25, 1990.

0022-0841/91/6101-0873$12.50

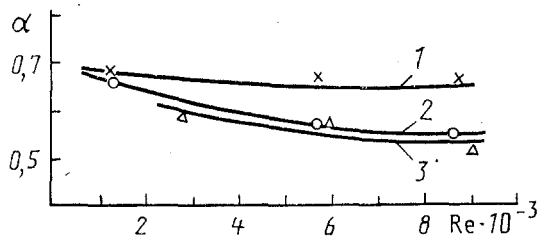

Fig. 2. Flow coefficient α as a function of Reynolds number Re (β = 30°); 1) $d_0 = 6.5 \cdot 10^{-3}$ m; 2) $d_0 = 2 \cdot 10^{-3}$ m (circular holes); 3) $d_s = 3.75 \cdot 10^{-3}$ (slots).

ference ΔP between the outside and inside together with a known flow coefficient α. We have made measurements on how the working and design parameters affect the flow coefficient and pressure difference, from which we compared the experimental ΔP with the theoretical ones.

It is difficult to calculate the flow coefficient for a hole when the liquid travels as a spiral film on the inner wall and escapes perpendicular to the motion because gas and liquid escape from the holes together, so the experiments were performed with a spiral liquid flow without gas, for which purpose a cylinder of smaller diameter was inserted coaxially with a vorticizer in the lower part to spiralize the liquid, with the flow coefficient determined from the volume of liquid from the holes and the pressure difference. We used water with an element 50 × 2.5 mm in diameter, with the width of the annular channel $2.5 \cdot 10^{-3}$ m, number of blades 12, blade inclination 30°. The holes were located at a distance equal to the diameter of the element from the vorticizer.

Figure 2 shows how the spiral flow speed affects the flow coefficient. There is a certain fall in α for the holes and slots as the speed increases. The Reynolds number (abscissa) was defined from the equivalent diameter of the annular channel, while the velocity was the mean flow speed based on the blade inclination, i.e., $w = L/(S \sin \beta)$, in which L is the liquid flow in m^3/sec, S the channel area in m^2, and β the blade inclination in degrees.

We measured the pressure differences due to the spiraling flow with a water–air system as follows: mean flow velocity w_0 in an element 10-20 m/sec, irrigation density q = 0.12-0.57 kg/m·sec (this corresponds to Re_f = 490-2280), β 30-60°; and ratio of distance of holes from vorticizer to internal diameter x/d = 1.3-2.5. The last of these was taken as 0.045 m. The pressure exerted by the flow was measured with a piezometer, while the pressure outside the element was atmospheric.

Figure 3 shows that there was no appreciable variation in ΔP in the x/d range used, nor was there any large effect from Re_f. The pressure differences for the dry element differed little from those for the irrigated one, so one can take ΔP for the latter as for the former. The separating elements work with comparatively low liquid loads, so this is justified.

The pressure difference as a function of dimensionless quantities affecting the value was fitted to

$$\Delta P = \exp(A)\,\mathrm{Re}^a\,\mathrm{Re}_f^b \left(\frac{x}{d}\right)^c, \quad \text{Pa.} \tag{1}$$

The coefficients and exponents in (1) are given in Table 1 for various β.

The mean relative deviation between the (1) ΔP and the observed values was 3.5% (β = 30°), 20% (β = 45°), and 15% (β = 60°).

As the pressure difference was only slightly dependent on Re_f, and the irrigated values were only slightly different from the dry ones, one can calculate ΔP on the assumption that it is related only to the tangential component u_φ of the total velocity vector for the gas. The gas velocity profile in the cylinder in dimensionless terms is $u_\varphi = f(\bar{r})$, $u_{0c} = f(\bar{r})$, $u_\varphi^+ = u_\varphi/w_0$, $u_{0c}^+ = u_z/w_0$ and $\bar{r} = r/R$, which remain constant along the channel, and also $\partial/\partial\tau \equiv 0$ and $\partial/\partial\varphi \equiv 0$. We solved this from the Navier–Stokes equation with the gravitational force deleted and neglecting the continuity in the steady-state motion of the gas flow in the cylindrical coordinate system [3]:

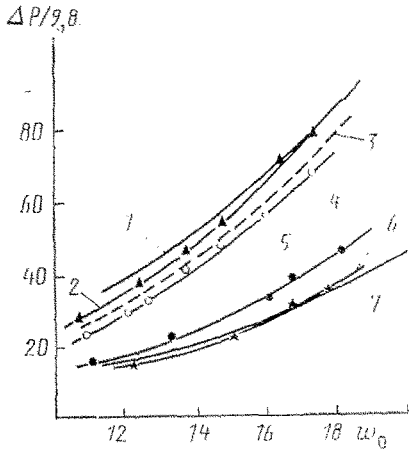

Fig. 3. Effects of gas–liquid loading on pressure difference: 2) x/d = 1.5, Re_f = 494.4, β = 30°; 3) 1.9; 0 and 30°; 4) 2.5; 494.4 and 45°; 5) 1.9; 494.4 and 45°; 6) 2.5; 494.4 and 45°. Calculated values from (12): Re_f = 0, x/d = 1.9, 1) β = 30°; 7) β = 45°. ΔP/9.8 N/m; w_0, m/sec.

TABLE 1. Coefficient in Eq. (1)

A	a	b	c	β, deg
−16.017	2.11	−0.02	−0.35	30
−5.67	0.47	1.0	−0.44	45
−2.46	0.42	0.45	−1.1	60

$$\rho\left(u_r\frac{\partial u_r}{\partial r}-\frac{u_\varphi^2}{r}\right)=-\frac{\partial P}{\partial r}+\mu\left(\frac{\partial^2 u_r}{\partial r^2}+\frac{1}{r}\frac{\partial u}{\partial r}-\frac{u_r}{r^2}\right), \tag{2}$$

$$\rho\left(u_r\frac{\partial u_\varphi}{\partial r}+\frac{u_r u_\varphi}{r}\right)=\mu\left(\frac{\partial^2 u_\varphi}{\partial r^2}+\frac{1}{r}\frac{\partial u_\varphi}{\partial r}-\frac{u_\varphi}{r^2}\right), \tag{3}$$

$$\frac{\partial u_z}{\partial z}+\frac{1}{r}\frac{\partial}{\partial r}(ru_r)=0. \tag{4}$$

The radial velocity component u_r is small, so it is usually neglected [4, 5]: $u_r = 0$, and then (4) implies $\partial u_z/\partial z = 0$, which means that the profile for the axial component does not vary along the cylinder. These conditions correspond to short tubes and have been confirmed by experiment [4]. Then (2) and (3) become

$$\frac{dP}{dr}=\rho\frac{u_\varphi^2}{r}, \tag{5}$$

$$\frac{d^2u_\varphi}{dr^2}+\frac{1}{r}\frac{du_\varphi}{dr}-\frac{u_\varphi}{r^2}=0. \tag{6}$$

The general solution to the latter is

$$u_\varphi=c_1r+c_2/r.$$

The boundary conditions are

$$u_\varphi=0 \quad \text{if} \quad r=R, \tag{7}$$

$$\overline{u}_\varphi=\frac{1}{\pi R^2}\int_0^R u_\varphi 2\pi r dr=2\int_0^1 u_\varphi\bar{r}d\bar{r}, \tag{8}$$

in which $\bar{r} = r/R$.

Then (7) gives

$$u_\varphi = c\left(\frac{1}{\bar{r}} - \bar{r}\right).$$

The finite u_φ near the axis implies $c_2 = 0$. Then $u_\varphi = c_1 r$, and the tangential component is

$$u_\varphi = \begin{cases} c_1\bar{r}, & 0 \leqslant \bar{r} < \bar{r}_0, \\ c\left(\dfrac{1}{\bar{r}} - \bar{r}\right), & \bar{r}_0 \leqslant \bar{r} \leqslant 1. \end{cases} \tag{9}$$

The function has its maximum for $\bar{r} = \bar{r}_0$. The continuity condition gives

$$u_\varphi = \begin{cases} c\left(\dfrac{1}{\bar{r}_{\max}^2} - 1\right)\bar{r}, & 0 \leqslant \bar{r} < \bar{r}_{\max}, \\ c\left(\dfrac{1}{\bar{r}} - \bar{r}\right), & \bar{r}_{\max} \leqslant \bar{r} \leqslant 1 \end{cases} \tag{10}$$

($\bar{r}_{\max}$ is the r corresponding to maximum u_φ).

We derive c from (8) to get

$$u_\varphi = \begin{cases} \dfrac{3}{4}\bar{u}_\varphi \dfrac{1 + \bar{r}_{\max}}{\bar{r}_{\max}^2}\bar{r}, & 0 \leqslant r < \bar{r}_{\max}, \\ \dfrac{3}{4}\dfrac{\bar{u}_\varphi}{1 - \bar{r}_{\max}}\left(\dfrac{1}{\bar{r}} - \bar{r}\right), & \bar{r}_{\max} \leqslant \bar{r} \leqslant 1. \end{cases} \tag{11}$$

We substitute (11) into (5) and integrate the latter to get the pressure at the wall created by the spiral gas flow:

$$P = \rho \int_0^1 \frac{u_\varphi^2}{\bar{r}}\, d\bar{r} = \frac{9}{16}\rho\bar{u}_\varphi^2\left(1 + \frac{1}{\bar{r}_{\max}} + \frac{1}{2\bar{r}_{\max}^2} + 2\ln\bar{r}_{\max} - \frac{\bar{r}_{\max}^2}{2}\right). \tag{12}$$

When the maximum lies near the wall, i.e., $\bar{r}_{\max} \approx 1$:

$$u_\varphi = \frac{3}{2}\bar{u}_\varphi\bar{r} \text{ and } P = \frac{9}{8}\rho\bar{u}_\varphi^2. \tag{13}$$

The tangential component $\bar{u}_\varphi$ of w_0, the mean flow rate velocity for the gas, is dependent on the latter and the spiraling angle in the static vorticizer. One assumes

$$\bar{u}_\varphi = w_0 \operatorname{tg}(k\beta), \tag{14}$$

in which k incorporates the deviation in the spiral angle of the flow from the blade inclination. Then one determines $\bar{r}_{\max}$ from the observed distributon for the tangential component over the cross section with a fixed blade angle and derives k from the experiments to use (12) to calculate P. In our case, the elements with blade vorticizers gave $\bar{r}_{\max} \approx 0.9$, k = 0.83.

Figure 3 compares the measurements with the (12) values, which agree satisfactorily in the range used.

Formulas have been derived for the characteristics that influence the liquid flow through the holes in separators and thus for the separation performance.

As the blade angle increases, the separation performance decreases substantially, so that angle should not be more than 30-35°.

These results can be used for analogous separation devices containing spiral gas–liquid flows.

NOTATION

d, element diameter; d_e, equivalent annular channel diameter; w and w_0, mean flow-rate velocities for liquid and gas; x, distance from holes to vorticizer; ΔP, pressure difference; u_φ, u_z, and u_r, tangential, axial, and radial gas flow velocities; r and R, current radius and element radius; τ, time; q, irrigation density; α, flow coefficient; β, blade inclination; ρ and ρ_ℓ, densities of gas and liquid; μ and μ_ℓ, dynamic viscosities of gas and liquid; $Re_f = 4q/u_\ell$, Reynolds number for liquid film; $Re = wd_e\rho_\ell/\mu_\ell$, Reynolds number for liquid in annular channel; d_0, diameter of holes; d_s, equivalent slot diameter.

LITERATURE CITED

1. V. M. Ramm, Gas Absorption, 2nd edn. [in Russian], Moscow (1976).
2. V. K. Shchukin, Heat Transfer and Hydrodynamics for Interior Flow under Mass Forces [in Russian], Moscow (1980).
3. L. G. Loitsyanskii, Liquid and Gas Mechanics [in Russian], Moscow (1987).
4. M. A. Gol'dshtik, Vortex Flows [in Russian], Novosibirsk (1981).
5. A. N. Nikolaev and V. A. Malyusov, Teor. Osnovy Khim. Tekh., 23, No. 2, 216-222 (1989).

VARIABLE-PRESSURE CAPILLARY IMPREGNATION OF A GAS-SATURATED POROUS MEDIUM

A. N. Shandrygin

UDC 532.68:622.279

Variable-pressure impregnation of a gas-saturated porous medium differs considerably from the constant-pressure case. The periodic pressure falls and rises have marked effects on the gas content. Pressure cycling can increase the extent to which the gas is displaced.

Tests have been made [1-3] on the effects of cyclic pressure on oil-saturated jointed porous collectors; that treatment raises the performance in capillary displacement.

The effects of cyclic pressure variation on capillary impregnation for a gas-saturated porous medium in experiments on various rocks have been examined. The cylinders were cut from natural sandstones and limestones and also from an artificial porous medium made of cement stone. The diameters were 0.0198-0.0204 m and the lengths 0.02-0.034 m. The permeability coefficients ranged from 0.005 to 8.9 μm^2, while the porosities varied from 49.9 to 30.6%. The water uptake was measured by a volumetric method, which in some cases was checked by weighing.

One-dimensional countercurrent and direct-flow methods were used. The specimens were prepared as in [4], but the residual water saturation was not simulated. In direct flow, the sides of the cylinders were coated with epoxide resin, while in counterflow simulation, one of the ends was also treated with resin. The pressure variation was simulated by evacuating the cylinders. Various values were used for the pressure variation, the cycle time, and the time from the start of impregnation to the start of the cyclic treatment.

Pressure variation influenced the gas displacement, particularly the gas extraction and gas content coefficients. The gas-extraction coefficient was the ratio of the extracted gas volume to the initial gas volume in the specimen. The current gas saturation coefficient was defined as the ratio of the pore volume occupied by the gas to the total. There is a general similarity in the impregnation of low-porous and high-porous cylinders, but the time scales differ.

Millionshchikov Groznyy Petroleum Institute. Translated from Inzhenerno-Fizicheskii Zhurnal, Vol. 61, No. 1, pp. 88-91, July, 1991. Original article submitted June 4, 1990.